Electronic Supplementary Material (ESI) for Physical Chemistry Chemical Physics.

Rational Design of Formamidine Tin Based Perovskite Solar Cell with 30% Potential Efficiency via 1-D Device Simulation

Kaiwen Liang[a], Like Huang[a,b,*], Tianzhou Wang[a], Chaofeng Wang[a], Yi Guo[a], Yunliang Yue[c], Xiaohui Liu[a], Jing Zhang[a], Ziyang Hu[a], Yuejin Zhu[a,*]

[a]Department of Microelectronic Science and Engineering School of Physical Science and Technology, Ningbo University, Fenghua Road 818, Ningbo 315211, China

[b]National Laboratory of Solid State Microstructures, Nanjing University, Nanjing 210093, China.

[c]School of Information Engineering, Yangzhou University, Yangzhou 225127, China

Corresponding author. L. Huang, Y. Zhu
E-mail: huanglike@nbu.edu.cn; zhuyuejin@nbu.edu.cn

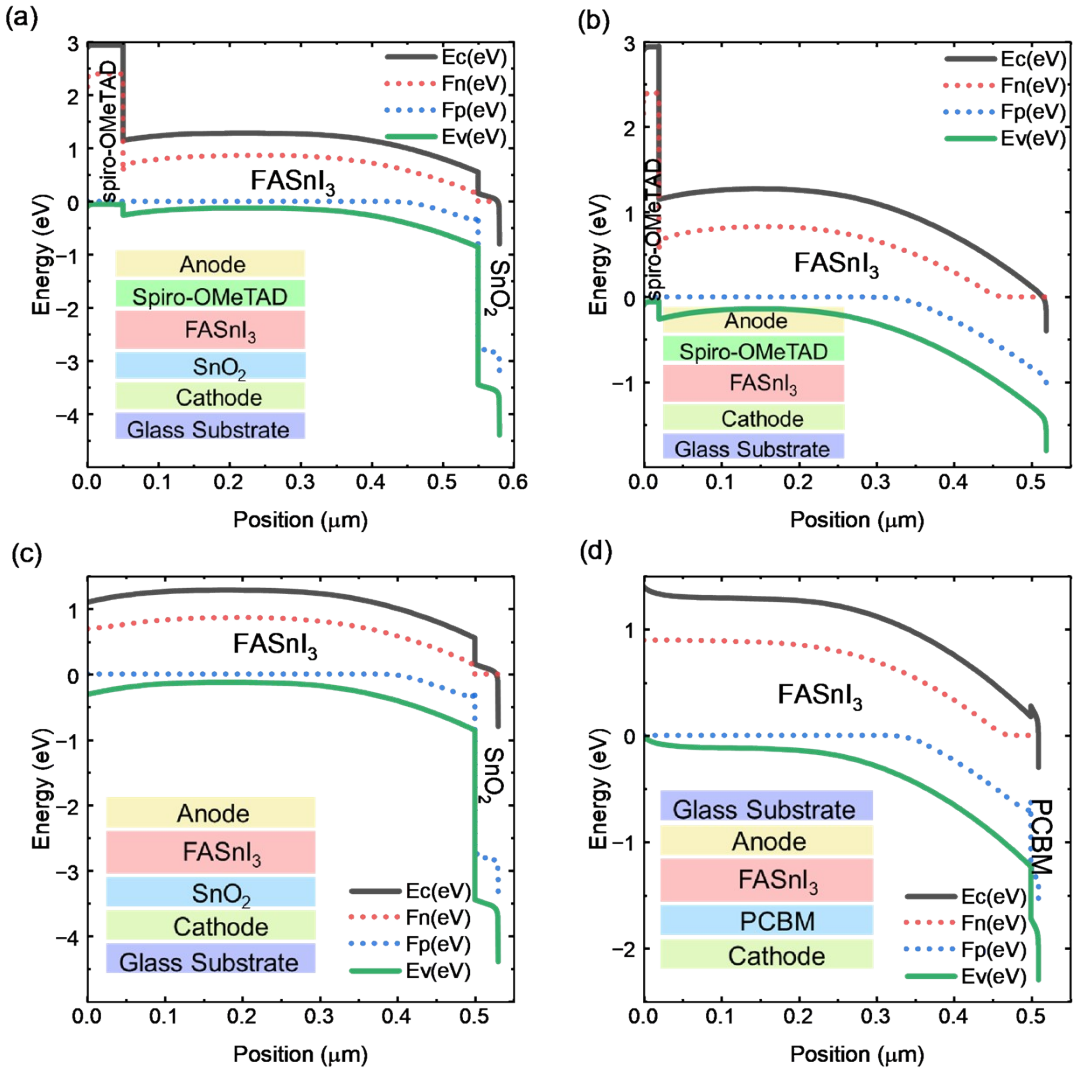

Fig. S1 The energy band diagrams of (a) n-i-p, (b) ETL-free, (c) HTL-free, and (d) inverted HTL-free PSCs are simulated with the initial parameters.

The energy band diagrams with the initial parameters are shown in Fig. S1. The absorber doping is p-type doping with an initial concentration of 1×10^{16} cm^{-3}. The valence band offset (VBO) is defined by equation (s-1), which denotes the difference between the valence band (VB) level of HTL and that of the absorber layer.

$$\mathrm{VBO} = E_{\mathrm{v\ (HTL)}} - E_{\mathrm{v\ (Absorber\ Layer)}} \qquad \text{(s-1)}$$

Here, $E_{\mathrm{v\ (HTL)}}$ denotes the VB level of HTL, and $E_{\mathrm{v\ (Absorber\ Layer)}}$ denotes the VB level of the absorber layer. When the VB energy level of the absorber layer is lower than that of HTL, the VBO is negative. It causes the formation of an energy cliff between the absorber and HTL. The energy cliff can boost hole transport to HTL from the absorber

layer.[1] As Fig. 2 shows, we can find that the VBO between spiro-OMeTAD and the absorber layer is -0.21 eV.

The conduct band offset (CBO) is defined by equation (s-2), which represents the difference between the conduction band (CB) level of ETL and that of the absorber layer.

$$\mathrm{CBO} = E_{\mathrm{c\ (Absorber\ Layer)}} - E_{\mathrm{c\ (ETL)}} \qquad \text{(s-2)}$$

Here $E_{\mathrm{c\ (Absorber\ Layer)}}$ denotes the CB level of the absorber layer, $E_{\mathrm{c\ (ETL)}}$ denotes the CB level of ETL. When the energy level of ETL is lower than that of the absorber layer, the CBO becomes negative. As Fig. 2 shows, the CBOs are -0.4 eV (SnO_2) and 0.1 eV (PCBM). The negative CBO is beneficial for electron transport to ETL from the absorber layer due to the formation of the energy cliffs between the absorber layer and ETL. Likewise, a small cliff is beneficial, but a large cliff improves the interfacial recombination, conducting in the deterioration of performance.

Table S1 The effects of the cathode electrode work function (WF) on the performance of n-i-p device.

WF of cathode (eV)	PCE (%)	V_{oc} (v)	J_{sc} (mA cm^{-2})	FF (%)
3.60	9.14	0.49	25.89	72.07
3.70	9.14	0.49	25.89	72.07
3.80	9.14	0.49	25.89	72.07
3.90	9.14	0.49	25.89	72.07
4.00	9.13	0.49	25.89	72.07
4.10	9.13	0.49	25.89	72.07
4.20	9.13	0.49	25.89	72.07
4.30	9.12	0.49	25.88	72.06
4.40	9.05	0.49	25.87	71.98
4.50	8.65	0.47	25.79	71.32

Table S2 The effects of the anode electrode WF on the performance of n-i-p device.

WF of anode (eV)	PCE (%)	V_{oc} (v)	J_{sc} (mA cm^{-2})	FF (%)
4.60	1.83	0.48	24.09	15.84
4.70	3.72	0.49	24.88	30.59
4.80	5.82	0.49	25.34	46.93
4.90	7.92	0.49	25.70	62.91
5.00	9.04	0.49	25.87	71.35
5.10	9.14	0.49	25.89	72.07

5.20	9.14	0.49	25.89	72.11
5.30	9.14	0.49	25.89	72.11
5.40	9.14	0.49	25.89	72.11
5.50	9.14	0.49	25.89	72.11

Table S3 The effects of the cathode electrode WF on the performance of n-i-p ETL-free device.

WF of cathode (eV)	PCE (%)	V_{oc} (v)	J_{sc} (mA cm^{-2})	FF (%)
3.60	20.98	0.96	27.98	77.98
3.70	20.98	0.96	27.98	77.98
3.80	20.98	0.96	27.98	77.97
3.90	20.97	0.96	27.97	77.95
4.00	20.86	0.96	27.91	77.76
4.10	20.35	0.94	27.78	77.62
4.20	18.78	0.86	27.63	78.60
4.30	16.50	0.77	27.46	78.36
4.40	14.07	0.67	27.28	77.35
4.50	11.64	0.57	27.06	75.91

Table S4 The effects of the anode electrode WF on the performance of n-i-p ETL-free device.

WF of anode (eV)	PCE (%)	V_{oc} (v)	J_{sc} (mA cm^{-2})	FF (%)
4.60	12.28	0.67	27.44	67.16
4.70	14.70	0.77	27.61	69.50
4.80	17.16	0.87	27.77	71.37
4.90	19.55	0.95	27.90	73.58
5.00	20.87	0.96	27.98	77.56
5.10	20.98	0.96	27.98	77.98
5.20	20.99	0.96	27.98	78.00
5.30	20.99	0.96	27.98	78.00
5.40	20.99	0.96	27.98	78.00
5.50	20.99	0.96	27.98	78.00

Table S5 The effects of the cathode electrode WF on the performance of n-i-p HTL-free device.

WF of cathode (eV)	PCE (%)	V_{oc} (v)	J_{sc} (mA cm^{-2})	FF (%)
3.60	9.06	0.49	25.70	72.08
3.70	9.06	0.49	25.70	72.08
3.80	9.06	0.49	25.70	72.08
3.90	9.06	0.49	25.70	72.08
4.00	9.06	0.49	25.70	72.08

4.10	9.06	0.49	25.70	72.07
4.20	9.06	0.49	25.70	72.07
4.30	9.05	0.49	25.70	72.06
4.40	8.98	0.49	25.69	71.98
4.50	8.58	0.47	25.60	71.34

Table S6 The effect of the anode electrode WF on the performance of n-i-p HTL-free device.

WF of anode (eV)	PCE (%)	V_{oc} (v)	J_{sc} (mA cm^{-2})	FF (%)
4.60	0.76	0.12	21.41	30.17
4.70	2.38	0.22	23.94	45.54
4.80	4.34	0.32	24.56	55.58
4.90	6.42	0.42	25.00	61.62
5.00	8.35	0.48	25.37	68.37
5.10	9.06	0.49	25.70	72.08
5.20	9.29	0.49	26.12	72.60
5.30	9.76	0.49	27.03	73.46
5.40	10.45	0.49	28.05	75.52
5.50	10.52	0.49	28.15	75.73

Table S7 The effects of the cathode electrode WF on the performance of p-i-n HTL-free device.

WF of cathode (eV)	PCE (%)	V_{oc} (v)	J_{sc} (mA cm^{-2})	FF (%)
3.60	9.14	0.49	25.89	72.07
3.70	9.14	0.49	25.89	72.07
3.80	9.14	0.49	25.89	72.07
3.90	9.14	0.49	25.89	72.07
4.00	9.13	0.49	25.89	72.07
4.10	9.13	0.49	25.89	72.07
4.20	9.13	0.49	25.89	72.07
4.30	9.12	0.49	25.88	72.06
4.40	9.05	0.49	25.87	71.98
4.50	8.65	0.47	25.79	71.32

Table S8 The effects of the anode electrode WF on the performance of p-i-n HTL-free device.

WF of anode (eV)	PCE (%)	V_{oc} (v)	J_{sc} (mA cm^{-2})	FF (%)
4.60	7.93	0.50	24.61	64.73
4.70	10.05	0.60	24.92	67.46
4.80	12.22	0.70	25.19	69.54
4.90	14.41	0.80	25.43	71.20

5.00	16.41	0.86	25.65	74.17
5.10	17.22	0.87	25.91	76.38
5.20	17.62	0.87	26.27	77.00
5.30	18.48	0.87	27.02	78.33
5.40	19.70	0.88	27.69	81.28
5.50	19.83	0.88	27.75	81.61

From Table S1-S8, when the WF of cathode electrode exceeds 4.3 eV, V_{oc}, J_{sc}, and FF will drop sharply and lead to lower efficiency. When this value is 3.6 eV, the best performance can be performed. Besides, better photovoltaic performance is achieved by increasing the WF of anode electrode. Finally, we varied the WF of cathode electrode to 3.6 eV and the WF of anode electrode to 5.1 eV, 5.4 eV, 5.5 eV, and 5.4 eV in four devices, obtained PCEs of 9.14 %, 20.99%, 10.52%, and 19.70%.

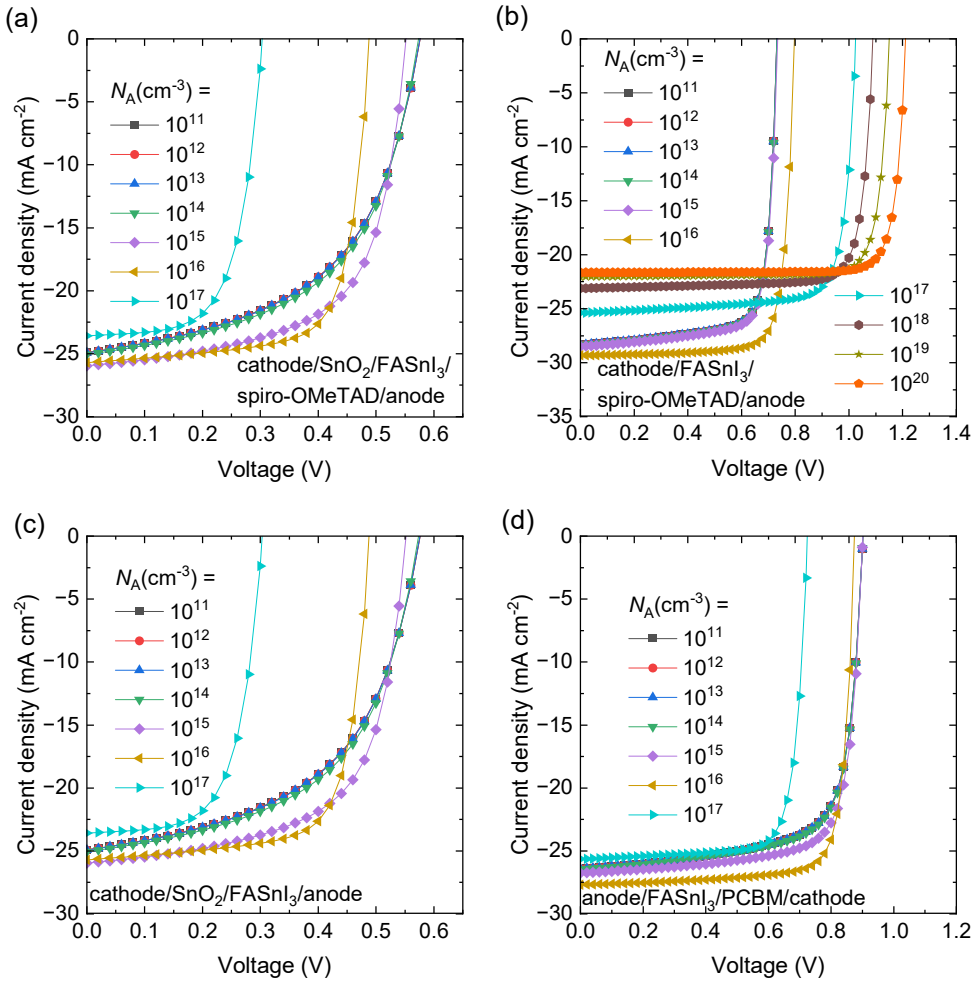

Fig. S2 The *J-V* curves with varying N_A of (a) n-i-p, (b) ETL-free, (c) HTL-free, and (d) inverted HTL-free devices, respectively.

From **Fig. S2** we can summarise the relationship of N_A to J_{sc} and V_{oc}. The specific changes in corresponding performance parameters are further shown in **Fig. 3**.

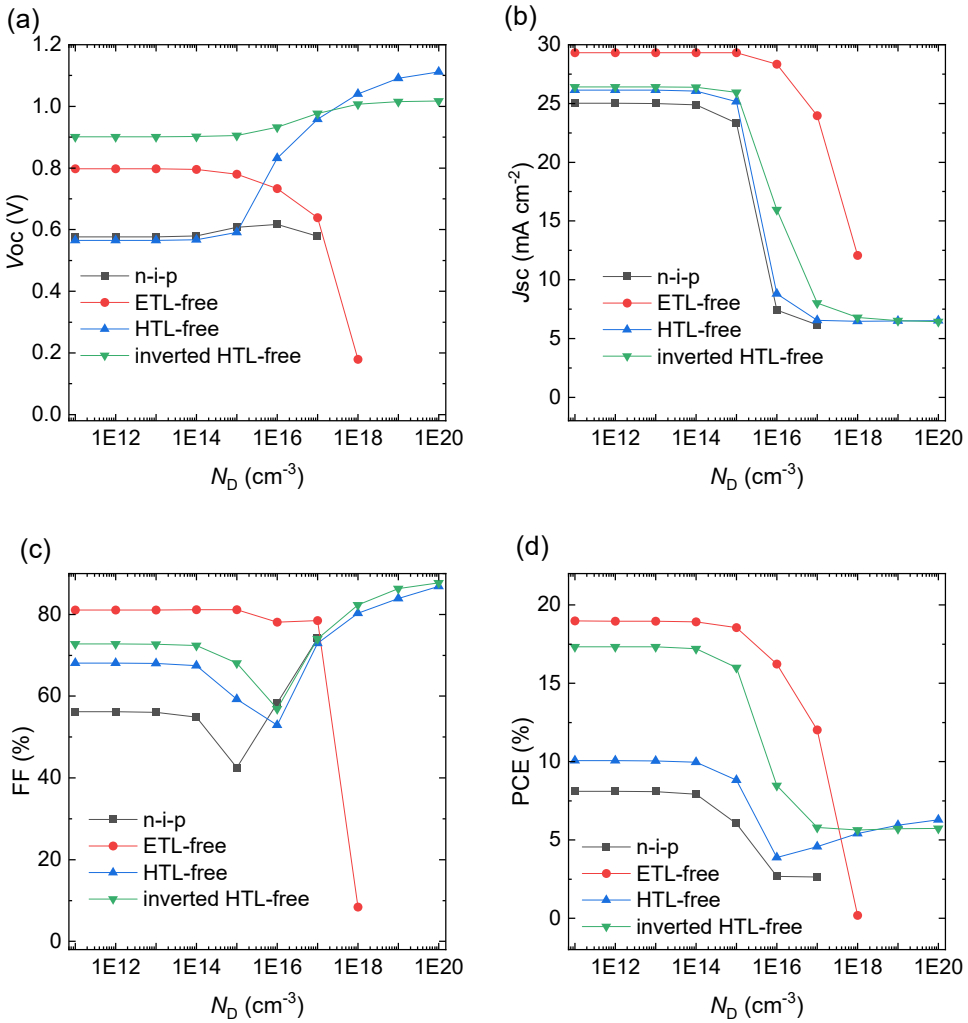

Fig. S3 (a) *V*oc, (b) *J*sc, (c) FF and (d) PCE as the function of N_D of the absorber layer in four devices.

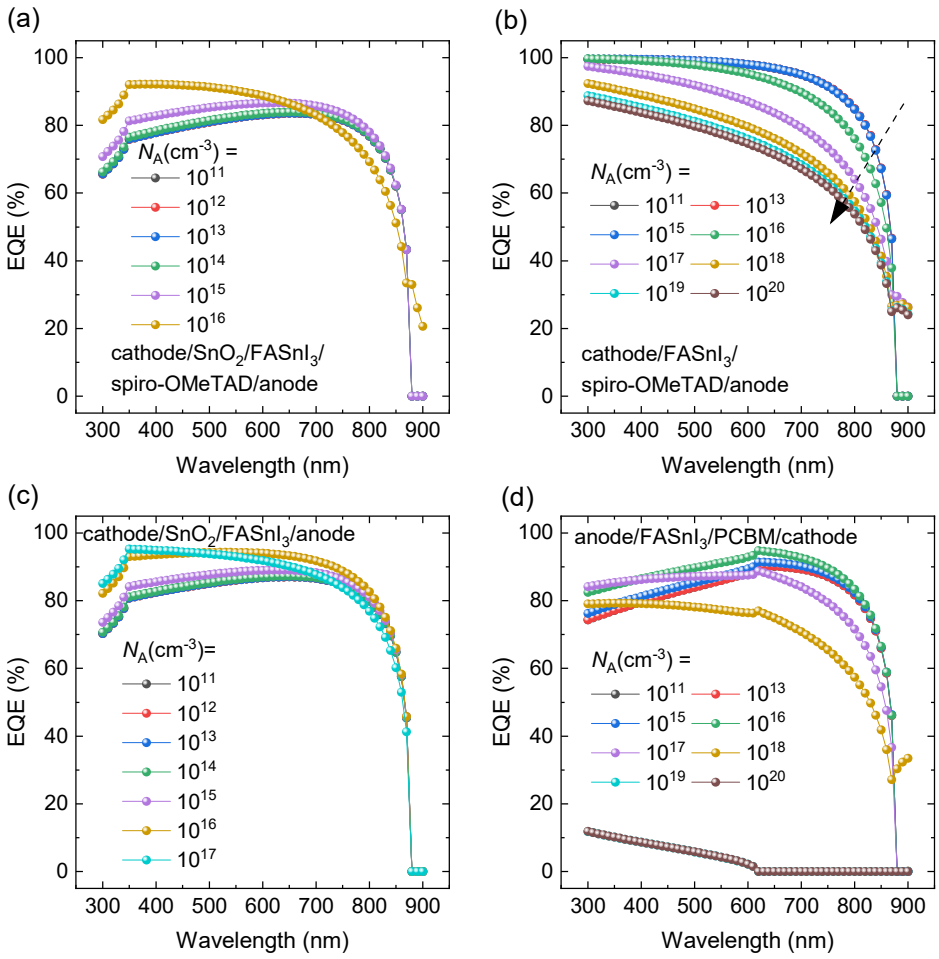

Fig. S4 The external quantum efficiency (EQE) with different absorber acceptor doping density (N_A) for (a) n-i-p, (b) ETL-free, (c) HTL-free, and (d) inverted HTL-free devices, respectively.

The EQE takes the optical performance of the solar cell along with the ratio of charge generation with respect to incident light photons. The EQE is calculated by equation (s-3):

$$\mathrm{EQE} = \frac{N_{\mathrm{electron}}}{N_{\mathrm{photon}}} = \frac{1240 \times J_{\mathrm{sc}}}{\lambda \times P_{\mathrm{in}}} \times 100\% \qquad \text{(s-3)}$$

Here, N_{electron} is the number of electrons obtained, N_{photon} is the number of incident photons, J_{sc} is the short-circuit current density of the PSCs in the case of monochromatic light irradiation, and λ is the wavelength of the incident light.[2]

From Fig. S4(a) and Fig. 3, as the N_A of n-i-p PSCs increases from 10^{11} cm^{-3} to 10^{15} cm^{-3}, the EQE of PSCs is enhanced, causing the increase of J_{sc}. However, as this value

increases to 10^{16} cm^{-3}, the EQE of the wavelength between 300 nm and 600 nm increase and decrease between 600 nm and 850 nm. As a result, the J_{sc} begins to drop after N_A exceeds 10^{16} cm^{-3}. Thanks to the increase of FF, it can be observed that the highest PCE of 9.38% was obtained when $N_A = 10^{16}$ cm^{-3}.

From Fig. Fig. S4(b) and Fig. 3, as the N_A of ETL-free PSCs increases from 10^{11} cm^{-3} to 10^{20} cm^{-3}, the EQE of the wavelength between 300 nm and 850 nm gradually decreases. PCE peaks only at $N_A = 10^{20}$ cm^{-3} due to continued growth of V_{oc} and FF.

From Fig. Fig. S4(d), as N_A of inverted HTL-free PSCs exceeds 10^{18} cm^{-3}, the EQE dramatically decreases below 10% and causes the J_{sc} to almost decrease to 0 mA cm^{-2}.

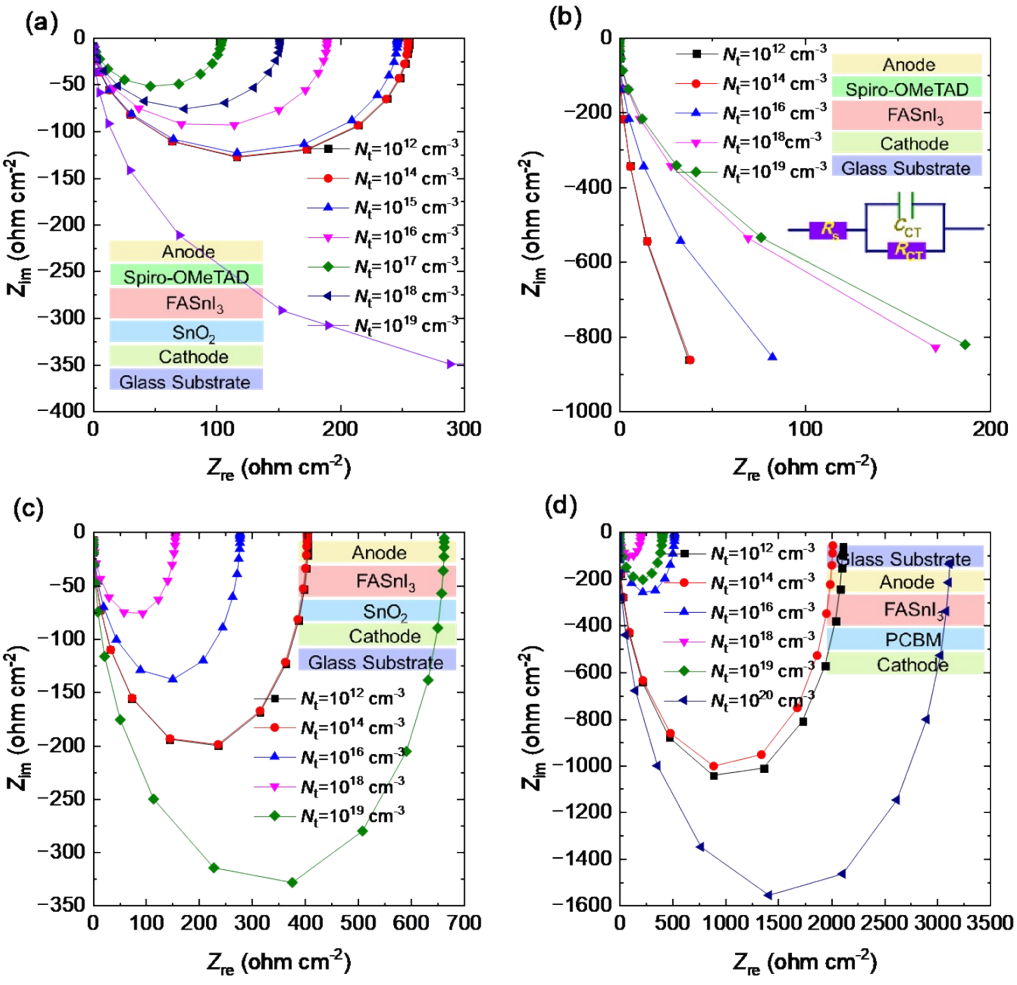

Fig. S5 The Nyquist plot with different absorber defect densities (N_t) for (a) n-i-p, (b) ETL-free, (c) HTL-free, and (d) inverted HTL-free devices, respectively.

The Nyquist plot with different absorber defect densities of four PSCs is shown in

Fig. S5. The plot represents the real and imaginary impedance of the simulated PSCs. It is used to determine the resistance to obtain the equivalent electrical circuit of the PSCs. The R_{ct} of n-i-p PSCs shown in Fig. S5(a) will decrease to about 50 Ω before the N_t increases to 10^{17} cm^{-3} and increase to over 75 Ω when it reaches 10^{18} cm^{-3}. Eventually, the R_{ct} will be over 350 Ω when N_t is 10^{19} cm^{-3}. Moreover, the R_{ct} of the HTL-free device (shown in Fig. S5(c)) will increase to 650 Ω when N_t reaches 10^{19} cm^{-3}. Besides, the R_{ct} of inverted HTL-free PSCs (shown in Fig. S5(d)) will decrease to nearly 100 Ω from approximately 1000 Ω when N_t reaches 10^{18} cm^{-3} and then increase to almost 1600 Ω when N_t is 10^{20} cm^{-3}. The lower charge-transfer resistance shows the smaller semicircle diameter of the Nyquist plot. The R_{ct} of n-i-p PSCs is much smaller than that of ETL-free, HTL-free, and inverted HTL-free devices. Therefore, the n-i-p structure is beneficial for carrier transport, which means a better structure to improve photovoltaic performance.[3]

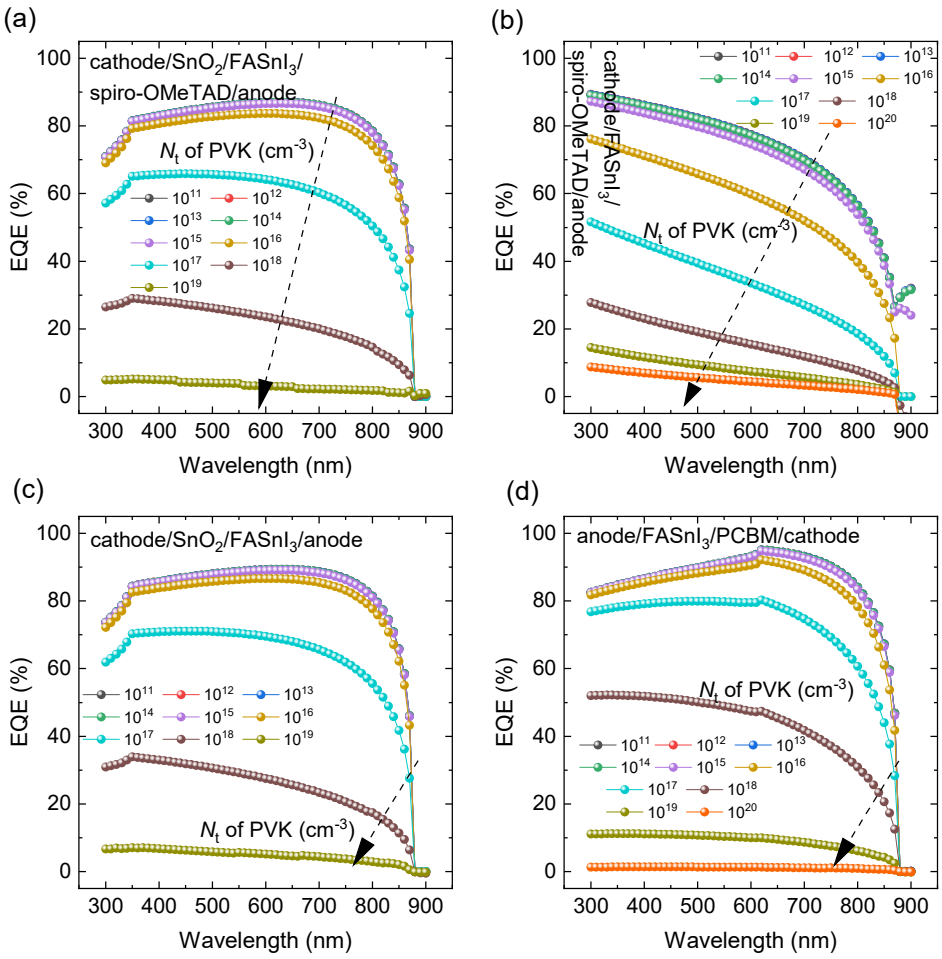

Fig. S6 The EQE with different N_t for (a) n-i-p, (b) ETL-free, (c) HTL-free, and (d) inverted HTL-free devices, respectively.

It can be observed that EQE decreases with increasing N_t in Fig. S6. Meanwhile, the change of EQEs is no longer apparent when $N_t < 10^{16}$ cm^{-3}. That explains why its effect on the PSCs' performance is almost negligible when $N_t < 10^{16}$ cm^{-3} in Fig. 7. The N_t of ETL-free PSCs with a threshold of 10^{15} cm^{-3} is lower than that of the other three devices. As a result, the optimal values of N_t are selected as 10^{12} cm^{-3} for PSCs as an ideal circumstance in simulation. However, the values can be relaxed to 10^{14} cm^{-3} for ETL-free PSCs, 10^{15} cm^{-3} for inverted HTL-free PSCs, and 10^{16} cm^{-3} for n-i-p, HTL-free PSCs in experiments. Changes in N_t within this range do not have a conspicuous impact on the performance of PSCs.

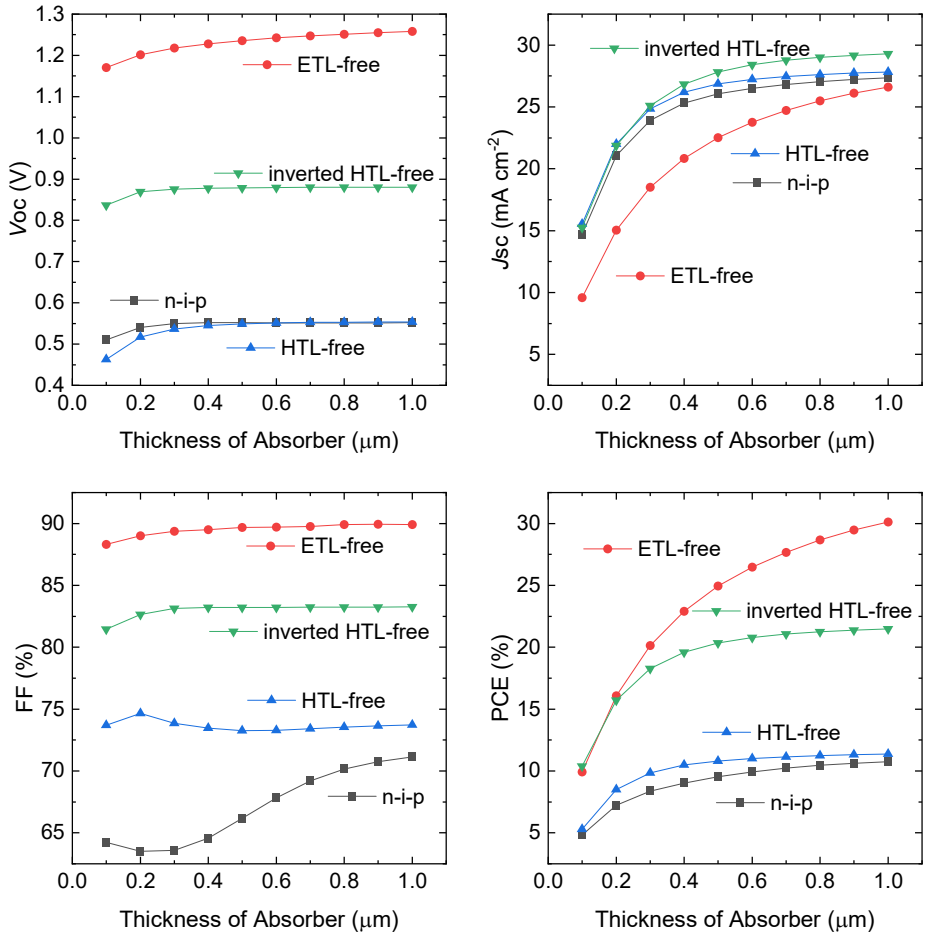

Fig. S7 The effect of absorber thickness on (a) V_{oc}, (b) J_{sc}, (c) FF and (d) PCE of four devices.

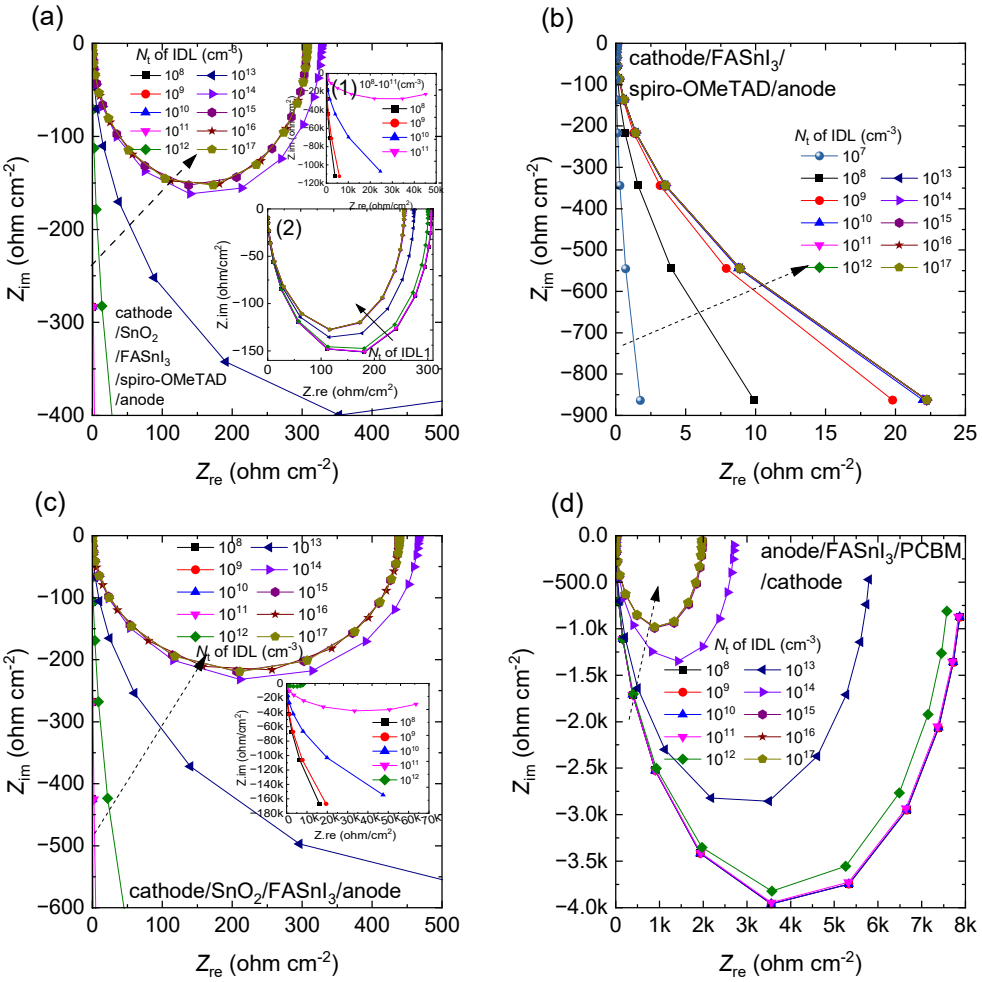

Fig. S8 The Nyquist plot with different interfacial defect densities (N_{it}) for (a) n-i-p, (b) ETL-free, (c) HTL-free, and (d) inverted HTL-free devices, respectively.

The Nyquist plot with different N_{it} of four PSCs is shown in Fig. S8. This is the representation of the real and imaginary impedance of the simulated PSCs. First, we look at the n-i-p structure. On the one hand, N_{it} of IDL1 does not have a significant effect on R_{ct}, which decreases from 300 Ω to 250 Ω as N_{it} increases from 10^8 cm^{-3} to 10^{17} cm^{-3}. On the other hand, the R_{ct} of n-i-p PSCs shown in Fig. S8(a) will decrease to about 325 Ω when the N_{it} of IDL2 increases to 10^{14} cm^{-3} and decrease to 300 Ω when it reaches 10^{15} cm^{-3}. Eventually, the R_{ct} will be stable at 300 Ω when $N_{it} > 10^{15}$ cm^{-3}. The simulated Nyquist plot of ETL-free PSCs does not form a complete semicircle, but we can observe that the plot arcs inward as N_{it} increases. Moreover, the R_{ct} of HTL-free device (shown in Fig. S8(c)) will decrease to 450 Ω when N_{it} increases to 10^{14} cm^{-3}.

Besides, the R_{ct} of inverted HTL-free PSCs (shown in Fig. S8(d)) will decrease to nearly 2600 Ω from approximately 6000 Ω when N_{it} reaches 10^{14} cm^{-3} and then stabilize at almost 2000 Ω when N_{it} increases to 10^{15} cm^{-3}. The lower charge-transfer resistance shows the smaller semicircle diameter of the Nyquist plot. It can be observed that the stability of PSCs is better when N_{it} is larger than 10^{14} cm^{-3}. However, since our calculation pursues higher efficiency than expected, 10^{14} cm^{-3} is not used as the final reference result. This problem needs to be paid attention to in the experiment. When N_{it} is equal to 10^{14} cm^{-3}, the PCEs of the four devices are 11.82%, 30.12%, 11.94%, and 22.49%, respectively.

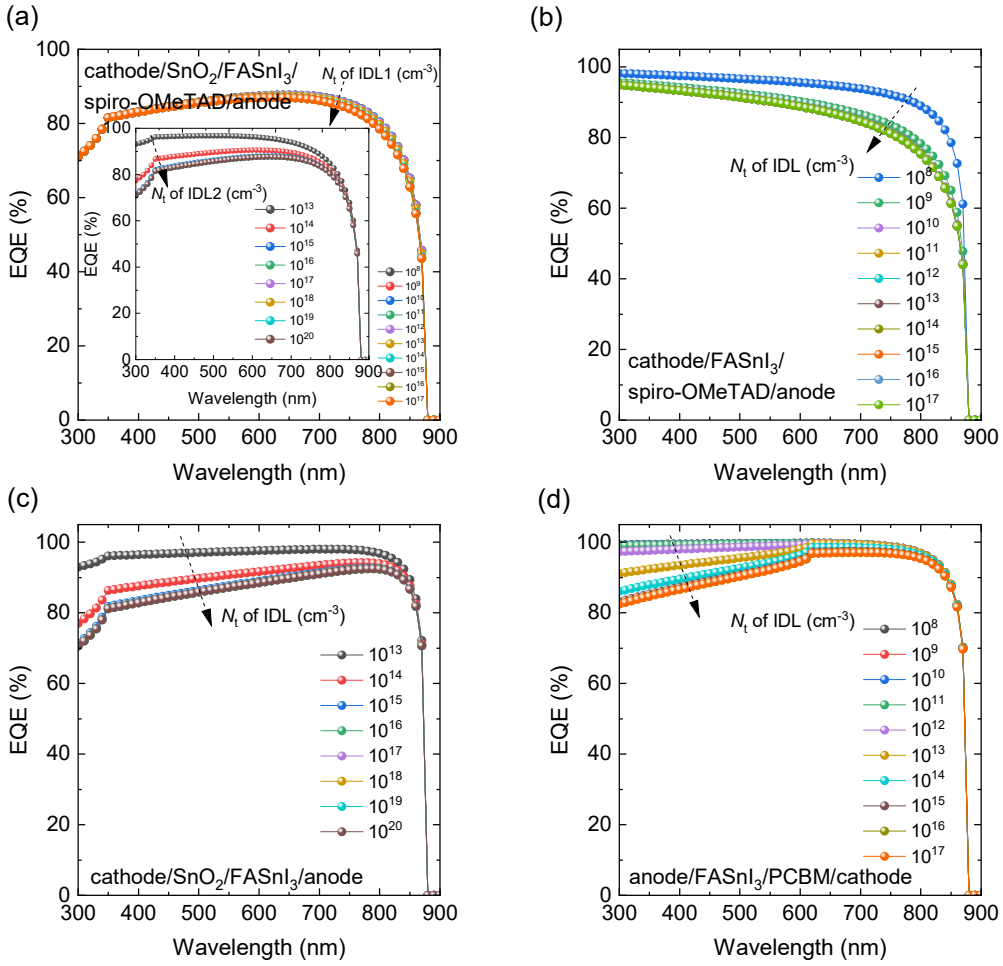

Fig. S9 The EQE with different N_{it} for (a) n-i-p, (b) ETL-free, (c) HTL-free, and (d) inverted HTL-free devices, respectively.

EQE is an important tool for characterizing the response of the PSC to different light spectra. The EQE allows for the identification of the spectral regions contributing to

the photocurrent generation of a solar cell. It is a key tool for characterizing the PSCs' response to different light spectra. Experimentally, the EQE can be determined using a monochromator and a light source, frequently a Xe lamp. Through a suitable shadow mask, the light source illuminates the sample. The device is kept in short-circuit condition, and a source meter is used to measure the current passing through the device for each wavelength.

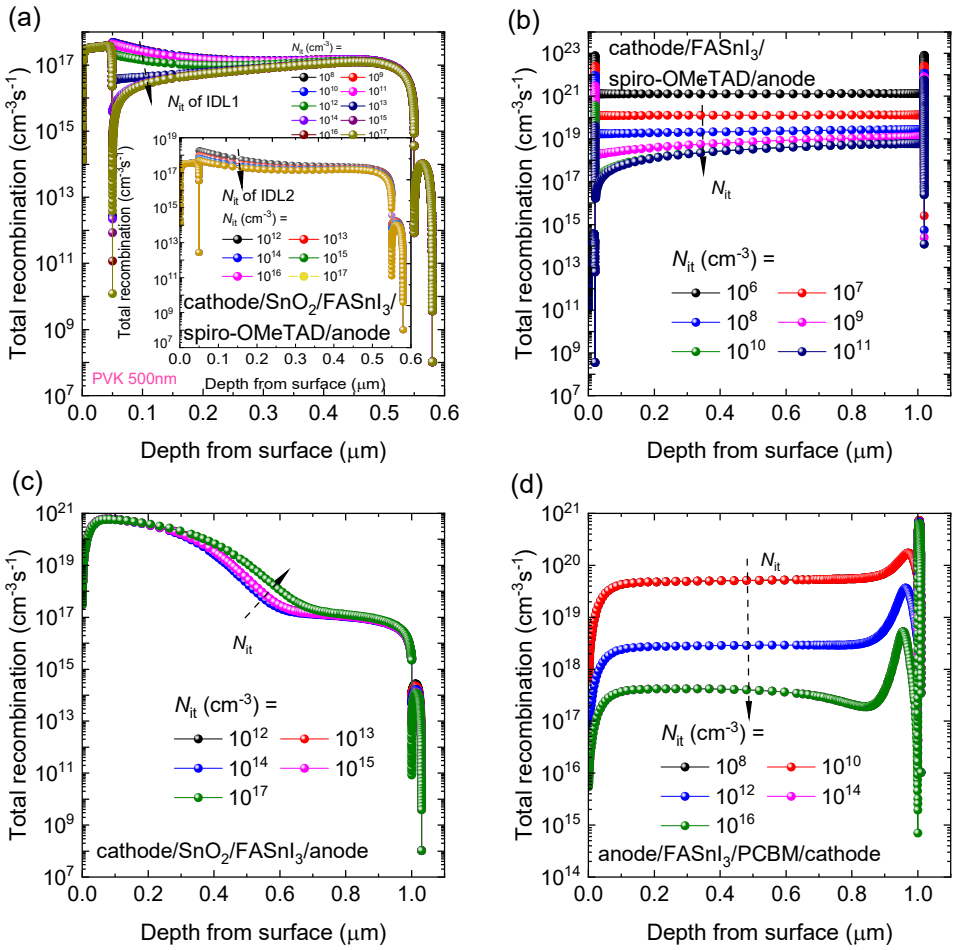

Fig. S10 The total recombination with different N_{it} for (a) n-i-p, (b) ETL-free, (c) HTL-free, and (d) inverted HTL-free devices, respectively.

Table S9 Optimized n-i-p PSCs' photovoltaic performance in each step.

Device parameters	Initial value	WF	Absorber layer				N_{it}
			N_A	N_D	N_t	thickness	
V_{oc} [V]	0.49	0.49	0.55	0.58	0.55	0.55	0.64
J_{sc} [mA cm^{-2}]	25.89	25.89	25.95	25.01	26.06	27.36	31.03
FF [%]	72.07	72.07	65.54	56.22	66.18	71.13	81.44

PCE [%]	9.14	9.14	9.38	8.11	9.52	10.74	16.10

Table S10 Optimized ETL-free PSCs' photovoltaic performance in each step.

Device parameters	Initial value	WF	Absorber layer			N_{it}
			N_A	N_t	thickness	
V_{oc} [V]	0.96	0.96	1.21	1.24	1.26	1.26
J_{sc} [mA cm^{-2}]	27.98	27.98	21.67	22.52	26.61	26.61
FF [%]	77.98	78.00	85.71	89.68	89.92	89.92
PCE [%]	20.98	20.99	22.51	24.96	30.12	30.12

Table S11 Optimized HTL-free PSCs' photovoltaic performance in each step.

Device parameters	Initial value	WF	Absorber layer			N_{it}
			N_A	N_t	thickness	
V_{oc} [V]	0.49	0.49	0.55	0.55	0.55	0.64
J_{sc} [mA cm^{-2}]	25.70	28.15	26.77	26.86	27.83	31.04
FF [%]	72.08	75.73	72.64	73.26	73.71	82.26
PCE [%]	9.06	10.52	10.67	10.81	11.36	16.26

Table S12 Optimized inverted HTL-free PSCs' photovoltaic performance in each step.

Device parameters	Initial value	WF	Absorber layer			N_{it}	N_D of PCBM
			N_A	N_t	thickness		
V_{oc} [V]	0.89	0.88	0.88	0.88	0.88	1.06	1.06
J_{sc} [mA cm^{-2}]	27.69	27.69	27.69	27.82	29.29	30.92	31.04
FF [%]	80.10	81.28	81.28	83.21	83.26	87.73	88.33
PCE [%]	19.70	19.70	19.70	20.34	21.47	28.83	29.10

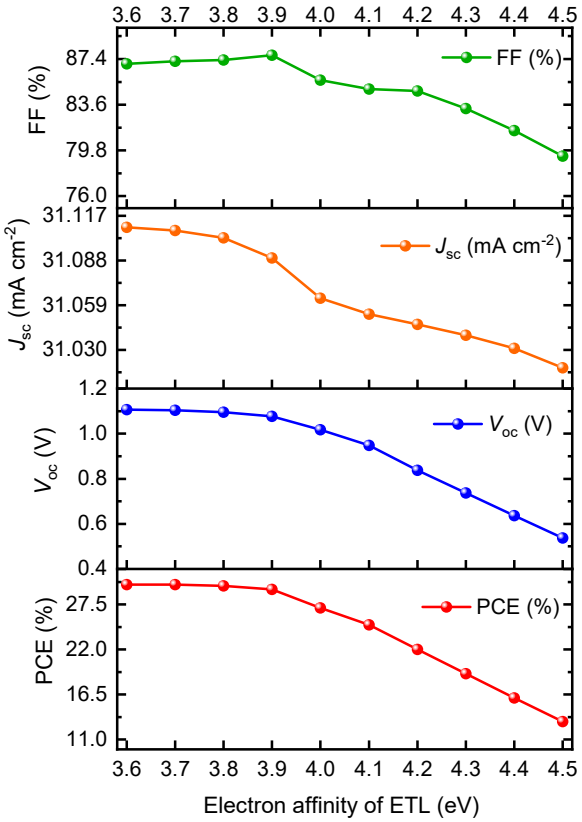

Fig. S11 The effect of ETL electron affinity on the n-i-p PSCs' performance.

The structure of simulated n-i-p PSCs is SnO_2/$FASnI_3$/spiro-OMeTAD. The CBO between SnO_2 and $FASnI_3$ is -0.4 eV in this study. A small cliff is beneficial, but a large cliff improves the interfacial recombination, conducting in the deterioration of photovoltaic performance. From **Fig. S11**, as the CBO between SnO_2 and $FASnI_3$ increases from -0.5 to 0.4, the PCE of PSCs increases from 13.21% to 29.94%.

References

1 Y. He, L. Xu, C. Yang, X. Guo, S. Li, *Nanomaterials (Basel)* 2021, **11**, 2321.

2 L. Hao, T. Li, X. Ma, J. Wu, L. Qiao, X. Wu, G. Hou, H. Pei, X. Wang, X. Zhang, *Opt. Quantum Electron.* 2021, **53**, 524.

3 M. Zhu, Q. Liu, W. Chen, Y. Yin, L. Ge, H. Li, K. Wang, *ACS Appl. Mater. Interfaces* 2017, **9**, 38832.